The Endosperm-Derived Embryo Sheath Is an Anti-adhesive Structure that Facilitates Cotyledon Emergence during Germination in Arabidopsis

Nicolas Doll, Simone Bovio, Angelo Gaiti, Anne-Charlotte Marsollier, Sophy Chamot, Steven Moussu, Thomas Widiez, Gwyneth Ingram

The endosperm-derived embryo sheath is an anti-adhesive structure that facilitates cotyledon emergence during germination in Arabidopsis.

N. M. Doll, S. Bovio, A. Gaiti, A-C. Marsollier, S. Chamot, S. Moussu, T. Widiez, G. Ingram.*

Laboratoire Reproduction et Développement des Plantes, University of Lyon, ENS de Lyon, UCB Lyon 1, CNRS, INRAE, F-69342, Lyon, France.

*Corresponding Author:
Gwyneth INGRAM
Laboratoire Reproduction et Développement des Plantes
ENS de Lyon,
46 Allée d'Italie
F-69342, Lyon, France.

Tel: 0033 4 72 72 86 02
Email :Gwyneth.Ingram@ens-lyon.fr

SUMMARY

Germination *sensu stricto* in Arabidopsis involves seed coat and endosperm rupture by the emerging seedling root. Subsequently the cotyledons emerge rapidly from the extraembryonic tissues of the seed, allowing autotrophic seedling establishment. Seedling survival depends upon the presence of an intact seedling cuticle that prevents dehydration, and which has hitherto been assumed to form the interface between the newly germinated seedling and its environment. Here we show that in Arabidopsis this is not the case. The primary interface between the emerging seedling and its environment is formed by an extra-cuticular endosperm-derived glycoprotein-rich structure called the sheath, which is maintained as a continuous layer at seedling surfaces during germination, and becomes fragmented as cotyledons expand. Mutants lacking an endosperm specific cysteine-rich peptide (KERBEROS (KRS)), show a complete loss of sheath production. Although *krs* mutants have no defects in germination *sensu stricto* they show a delay in cotyledon emergence, a defect not observed in seedlings with defects in cuticle biosynthesis. Biophysical analyses reveal that the surfaces of wild-type cotyledons show minimal adhesion to silica beads in an aqueous environment at cotyledon emergence, but that adhesion increases as cotyledons expand. In contrast *krs* mutant cotyledons show enhanced adhesion at germination. Mutants with defects in cuticle biosynthesis, but no sheath defects, show a similar adhesion profile to wild-type seedlings at germination. We propose that the sheath reduces the adhesiveness of the cotyledon surface under the humid conditions necessary for seed germination, and thus promotes seed coat shedding and rapid seedling establishment.

Keywords: Embryo, Endosperm, Surface, Adhesion, Germination, Cotyledon, Arabidopsis

RESULTS AND DISCUSSION

The embryo sheath, and not the cuticle, forms the primary interface with the environment upon cotyledon and hypocotyl emergence.

Arabidopsis seed development, is triggered by a double fertilization event that leads to the production of two tissues; the embryo (from the fertilized egg cell) and the endosperm (from the fertilized central cell of the female gametophyte). The coordinated development of these two tissues is critical for the production of fully viable seeds. In Arabidopsis the initial growth of the seed is driven by the expansion of the endosperm, which is then progressively replaced by the invasively growing embryo. Only one viable layer of endosperm cells remains at seed maturity (reviewed in [1]). During this process a structure called the embryo sheath, composed of material rich in EXTENSIN epitopes, is produced in the endosperm surrounding the developing embryo and deposited at the embryo surface, outside the embryonic cuticle [2]. Sheath deposition correlates with an apparent reduction in the adhesion of the embryo to the endosperm during seed development both temporally and in a variety of backgrounds defective in sheath deposition, and facilitates the invasive growth of the embryo through the endosperm in developing seeds.

We tested whether the sheath remains within the seed at germination or whether it adheres to the seedling surface upon emergence. Immunolocalisations of resin sections with the anti-EXTENSIN JIM12 antibody [3] revealed that the newly emerged embryo-derived surfaces of wild-type seedlings at 2 Days After Stratification (DAS) are covered with a continuous sheath (Figure 1A). We previously reported [2], that this structure could also be detected with the LM1 anti-EXTENSIN antibody [4], and we could also detect it using the JIM19 anti-EXTENSIN antibody [3] (Figure S1). Previous work has shown that the KRS protein is necessary for sheath production. However a structure-function analysis suggested that KRS likely regulates sheath production rather than forming a structural component of the sheath [2]. Consistent with the previously reported absence of sheath production by the endosperm of developing *kerberos (krs)* mutant seeds, sheath material is absent at the surface of *krs* mutant seedlings (Figure 1D-F, Figure S1). This result was confirmed by whole-mount immunolocalisations with JIM12, which show a strong and continuous signal on all aerial parts of wild type seedlings at 2 DAS, but no signal in the *krs* background (Figure 1G,J). Finally, analysis of cotyledons by transmission

electron microscopy confirmed the presence of an extra-cuticular matrix, corresponding to the embryo sheath on the surface of wild-type seedlings at 2DAS (Figure 1M,O). This structure is entirely absent at the surface of *krs-3* seedlings (Figure 1 O,P). Consistent with the observation that the sheath is strictly seed-derived [2], JIM12 signal on the surface of wild-type seedlings was progressively fragmented as seedlings expanded. At 4 DAS, the sheath on the wild type cotyledons was discontinuous (Figure 1B), and at 7 DAS, only a few patches remained on the cotyledon surface (Figure 1C). These results were confirmed by whole mount immunolabelling in which the JIM12 signal decreased strongly in intensity during cotyledon expansion (Figure 1H,I). As expected, JIM12 signal was found to be absent on post embryonic structures such as leaf primordia (Figure 1A). In the primary root, occasional patches of sheath-like material were observed, which may be derived from the embryonic root apex (Figure S1).

These results show that the assumption [5–10] that the Arabidopsis seedling cuticle forms the primary interface between the seedling and the environment upon germination is false, and that this interface is, in fact, formed by the embryo sheath; an endosperm derived structure.

Sheath deposition and embryonic cuticle formation are genetically separable processes.

Our previous work, combined with the above results, suggest that the embryo sheath is tightly associated with the embryo cuticle, the structure commonly thought to impart specific physical properties to plant surfaces (reviewed in [11,12]). To identify backgrounds that would allow us to discriminate between the specific functions of these structures, we analysed cuticle integrity in *krs* mutant seedlings which lack the embryo sheath. Staining with the lipophilic dye auramine O showed that *krs* mutants have a continuous and apparently normal cuticle after germination (Figure 2A-D). As previously proposed the reported slight increase in permeability of the *krs* cuticle after germination may be due to mechanical damage at cotyledon tips sustained during development or emergence [2]. No endosperm debris was observed on the surface of *krs* seedlings during staining, indicating that although the embryo and endosperm show an abnormally tight association during seed development [2] this cuticle ultimately allows a clean separation of the embryo from surrounding endosperm tissues. The *krs* cuticle was also found to be

indistinguishable from that of wild-type seedlings later in cotyledon development (Figure 1M-P, Figure S1). We conclude that *krs* is only deficient for sheath deposition but not for cuticle establishment. In addition we investigated sheath production in a mutant reported to have a defect specifically in cuticle biosynthesis, the *glycerol-3-phosphate acyltransferase 4 and 8 (gpat4 gpat8)* double mutant [13,14]. As previously reported, *gpat4 gpat8* mutant seedlings do not completely lack an embryonic cuticle [13]. Nonetheless the cuticle of *gpat4 gpat8* mutants stains only very weakly at 2 and 4 DAS, consistent with the role of these enzymes in cutin biosynthesis (Figure 2E,F, Figure S1)[13,14]. It is important to note that the complete lack of an embryonic cuticle is thought to lead to early embryo lethality (reviewed in [12,15]). Sheath production and deposition is not affected in *gpat4 gpat8* and the sheath is maintained on the cotyledon surface post germination in this background (Figure 2G,H). Consistent with this, embryo-endosperm separation occurs normally in *gpat4 gpat8* mutants (Figure 2G). Our results suggest that this genetic background shows defects only in cuticle biosynthesis, but not in sheath deposition. Thus, embryo sheath deposition can be functionally separated from cuticle biosynthesis. The *gpat4 gpat8* and *krs* mutants therefore represent valuable tools to separate the function of the embryonic cuticle from that of the embryo sheath during germination.

The presence of an intact embryo sheath facilitates the emergence of cotyledons from the seed coat.

The germination of *krs*, *gpat4 gpat8* and WT seeds was observed. 48h after stratification, *krs* plantlets have a significantly higher frequency of retention of the cotyledons within the extra embryonic tissues of the seed than either WT or *gpat4 gpat8* mutants (Figure 3C-F). Kinetic analysis in three independent mutant alleles of *KRS* revealed a significant delay in cotyledon escape in the presence of sucrose (Figure 3C, Figure S2). This effect was amplified in the absence of sucrose (Figure 3E, Figure S3). However, radicle emergence was not delayed, showing that germination *stricto sensu* is not affected in *krs* mutants (Figure 3D,F Figure S2). The fact that *gpat4 gpat8* plantlets do not present defects in cotyledon escape, indicates that this phenotype is specifically caused by the absence of the embryo sheath rather than by cuticle defects. The dynamics of cotyledon escape were also assessed in dark-grown seedlings in which cotyledons do not expand dramatically (Figure 3 G-J). Similarly to a growth in presence of light, a delay in cotyledon escape was

observed in *krs* compared to the WT and *gpat4 gpat8.* At 4 (96h) DAS, cotyledons frequently remain inside the extra-embryonic tissues in *krs* seedlings but very rarely in WT and *gpat4 gpat8* (Figure 3G,H).).

Based on our results, we hypothesise that the sheath promotes robust cotyledon escape from the seed even in absence of significant cotyledon expansion, reinforcing the hypothesis that the sheath is involved in reducing adhesion of cotyledons to surrounding tissues, and in lubrication during seed coat shedding. In further support of this hypothesis we found that seed coat shedding in wild-type seedlings, and radicle emergence in either wild-type or *krs* mutants, were only weakly affected by restriction of water availability by increasing agarose concentrations in the media [16]. In contrast, a decrease in water availability increased seed coat retention in *krs* mutant (Figure S3 B-D). Similarly, germination on media with abnormally high or low pH increased seed-coat retention in *krs* mutants but only marginally affected cotyledon escape in wild-type (Figure S3 I-N).

The presence of an intact embryo sheath promotes robust plant establishment.

We found that, in the absence of sucrose, a significant proportion (around 20%) of *krs* mutants arrest before the first leaves appear (Figure 3 K-M, Figure S2C). Levels of seedling arrest were correlated with cotyledon trapping, suggesting that cotyledon trapping may impede the establishment of autotrophic growth (Figure 3N). Consistent with this idea, seedling arrest was not observed in the presence of sucrose (which attenuated, but did not abolish the cotyledon trapping phenotype of *krs* mutants), or on soil (Figure 3C-D, K and Figure S2C). To investigate further whether defects in *krs* mutants translate into altered fitness, we carried out competition assays between wild-type and *krs-3* seeds sown as mixed populations at very high density on soil. Under normal growth conditions (1 plant per pot) *krs* mutants show no delay in bolting compared to wild-type plants. Genotyping revealed that only 16.33% (+/- 2,05% n=3, 100 bolts per sample) of bolts produced under high density conditions were derived from *krs* mutants, suggesting that loss of KRS function significantly impacts plant establishment under these conditions.

Changes in the adhesive properties of the cotyledon surface correlate with the presence of an intact sheath.

The fact that the sheath is maintained on the surface of young seedlings provides an opportunity to measure the biophysical properties of surfaces with and without a sheath, and notably to assess the adhesive properties of these surfaces. To assess this parameter we used atomic force microscopy (AFM) with a spherical silica tip (as in [17,18]) . Initial scans were carried out to acquire the topography of the sample and to identify cells (Figure 4A). Smaller areas (10 x 10 μm^2) were then selected for the generation of 8 x 8 grids of force curves for adhesion measurements (Figure 4B)(see materials and methods). Several grids were generated per cotyledon. Under our conditions little, if any, adhesion was measured at the surface of wild-type cotyledons at 2 DAS, whereas at 5 DAS, higher levels of adhesion were observed. *krs* cotyledons showed similar values of adhesion at 2 DAS and 5 DAS, and these values were similar to those observed in wild-type cotyledons at 5 DAS (Figure 4C,D). This is likely due to the fact that *krs* mutant cotyledons at 2 and 5 DAS, and wild-type cotyledons at 5 DAS, all have surfaces composed of a similar cutin matrix. Similar results were observed on both the adaxial and abaxial surface of cotyledons (Figure S4), and we therefore concentrated on adaxial surfaces which, being slightly convex, are more accessible to measurement. As previously observed in cuticle staining experiments, AFM scans and scanning electron microscopy analysis showed the absence of endosperm debris at the cotyledon surface of *krs* mutants (Figure S4). Thus, the presence of an intact sheath correlates with reduced adhesion both temporally in wild-type seedlings, and in the *krs* mutant. (Figure 4C,D) (Figure S4). These results suggest that the sheath is less adhesive under hydrated conditions than the cuticle, which is considered to be a non-adhesive structure [19].

Consistent with the fact that *gpat4 gpat8* mutants produce a normal sheath, their properties were identical to those of wild-type seedlings at 2 DAS (Figure 4C). Interestingly however, at 5 DAS, the surface of *gpat4 gpat 8* mutant cotyledons tended to be less adhesive than that of wild-type and *krs* seedlings (Figure 4D). This could reflect changes in cuticle composition caused by, or compensating for, the loss of the products of the GPAT4 and GPAT8 enzymes at this developmental stage. Such compensatory alterations, have been reported in studies of other cuticle biosynthetic mutants [5,20–23].

In conclusion, our work reveals that, contrary to the situation at other aerial plant surfaces, the primary interface of the newly emerged Arabidopsis embryo with its

environment is not the cuticle, but the extra-cuticular endosperm-derived embryo sheath. We demonstrate that the sheath renders the embryo surface less adhesive under humid conditions, which likely explains its role in permitting the growth of the embryo through the endosperm during seed development, and in facilitating robust cotyledon escape from the seed coat. Our results highlight a previously unsuspected role for endosperm-derived apoplastic components in the emergence of cotyledons during germination, and in seedling establishment, and also have potentially important implications for understanding the interactions of germinated seedlings with their environment.

Author Contributions

N.M.D., A.G., S.B., A-C.M. S.C. and S.M. conducted the experiments, T.W. helped with supervision. G.I and N.M.D. designed the experiments and wrote the paper with input from all authors.

Acknowledgements

We would like to thank A. Lacroix, J. Berger, P, Bolland, H. Leyral and I. Desbouchages for assistance with plant growth and logistics, and A. Patole, S. Maurin, B. Martin-Sempore and C. Vial for administrative assistance. AG was funded by the Erasmus student network. N.M.D was supported by the French Agence National de Recherche (ANR- 17-CE20-0027 ; Mind the Gap)

Declaration of Interests

The authors declare no competing interests.

Main Figure Legends

Figure 1: The sheath is maintained on the seedling surface at germination before being fragmented by tissue expansion.

A-F) JIM12 immunolabelling on sections of seedlings. JIM12 labelling is shown in green and cell walls stained with fluorescent brightener 28 in blue. A) Section of 2 DAS wild type seedling. B) Section of 4 DAS WT cotyledon. C) Section of 7 DAS WT cotyledon. D) Section of 2 DAS *krs-3* seedling. E) Section of 4 DAS *krs-3* cotyledon. F) section of 7 DAS *krs-3* cotyledon. Scale bars = 100µm in A-F. cot = cotyledon, hyp = hypocotyl, fl = first leaf, eet =

extraembryonic tissues of the seed. G-L) JIM12 whole mount immunolabelling. JIM12 labelling is shown in green. G) 2 DAS WT seedlings. H) 4 DAS WT cotyledon. I) 7 DAS WT cotyledon. J) 2 DAS *krs-3* seedlings. K) 4 DAS *krs-3* cotyledon. L) 7 DAS *krs-3* cotyledon. Scale bars = 200µm in G-L. M-P) Transmission electron microscopy images on 2DAS seedlings. M,O) Col-0 seedling. N,P) *krs-3* seedling. ECW = epidermis cell wall, cut = cuticle, ES = embryo sheath. Scale bars = 1µm in M and N, = 200nm in O and P.

Figure 2: Sheath deposition and cuticle biosynthesis are genetically separable processes.

A-F) Auramine O staining of the cotyledon cuticle 2 DAS. Arrows indicate the cuticle A) in Col-0, B) magnification of A, C) in *krs-3*, D) magnification of C, E) in *gpat4 gpat8*, F) magnification of E. G-H) JIM12 immunolabelling on section in the *gpat4 gpat8* mutant. JIM12 signal is in green and cell walls are stained with fluorescent brightener 28 (in blue). cot = cotyledon, sc = seed coat, emb = embryo, end = endosperm. Scale bars = 20µm in A,C,E, 2µm in B,D,F and 50µm in G and H.

Figure 3: Absence of sheath leads to defective cotyledon emergence and induces a premature seedling arrest in the absence of sugar.

2 DAS Col-0 seedling, B) 2 DAS *krs-3* seedling with the two cotyledon inside the seed coats. C) Percentage of seedlings with escaped cotyledons at different times after stratification for Col-0, krs-3 and *gpat4 gpat8* lines. N = 3 (repetitions from independent mother plants), 100 seedlings per repetition. Seedlings were grown on MS plates supplemented with 0,5% sucrose. D) Percentage of radicle emergence in the same experiment as that shown in C. E) Percentage of seedlings with escaped cotyledons at different times after stratification for Col-0, *krs-3* and *gpat4 gpat8* lines. N = 3 (repetitions from independent mother plants), 100 seedlings per repetition. Seedlings were grown on MS plates lacking sucrose. F) Percentage of radicle emergence in the same experiment as that shown in E. G) 5 DAS etiolated Col-0 seedlings. H) 5 DAS etiolated *krs-3* seedlings with the two cotyledons inside the seed coats. I) Percentage of seedlings with escaped cotyledons at different times after stratification for Col-0, *krs-3* and *gpat4 gpat8* lines. N = 3 (repetitions from independent mother plants), 100 seedlings per repetition. Seedlings were grown in absence of light, on MS plates lacking sucrose. J) Percentage of radicle emergence in the same experiment as that shown in I. K) Quantification of seedling growth arrest (at 12

DAS) in different conditions for Col-0 and *krs-3.* L) Normally developing *krs-3* seedlings 12 DAS, grown on MS lacking sucrose M) *Krs-3* seedlings grown in same conditions as in L and showing failure to establish (seedling growth arrest). N) In black: percentage of seedling growth arrest in 5 groups of *krs-3* seedlings grown in the absence of sucrose and classified based on the timing of cotyledon escape from the seed coats. Seedling arrest was scored at 9 DAS. In light gray: overall percentage of seedlings in each group. N = 3 (repetitions from independent mother plants), 200 seedlings per repetition ** and * represent statistically significant differences (p-value < 0.01 and p-value < 0.05 respectively) obtained after one-way ANOVA and subsequent Tukey HSD tests. ns = non-significant (p-value > 0,05). Scale bars = 500µm in A and B, = 200µm in E and F, = 2mm in L and M. +/- SD are represented on each bar plot.

Figure 4: Absence of the sheath leads to altered adhesive properties at the cotyledon surface.

A) Large scale topographical maps of cotyledon surfaces were acquired in QI mode (scan size 90x90 or 100x100 µm) in order to identify cells and define regions for adhesion measurements. 4 smaller (10x10 µm) regions of interest were then selected for extracting force curves. B) In each region of interest 64 curves were performed and then analysed to measure the adhesion force. The approach curve is shown in blue and the retract curve in red. Adhesion corresponds to the difference between the minimum of the retract curve and the base line. C,D) Cotyledon adhesion measurements for the three genotypes described above at 2 DAS and 5 DAS respectively. Average adhesion scatter plot. Each dot corresponds to the average adhesion measured for 1 cotyledon. Average +/- SEM is indicated on each scatter plot. One-way ANOVA tests were performed for between-dataset comparisons, with an a-value of 0.05. *** indicates p-value ≤ 0.001, **** indicates p-value ≤ 0.0001, ns indicates p-value > 0.05 in a subsequent Sidak post-hoc test.

Supplementary Figure Legends

Figure S1: Supplementary analyses of seedling surface composition and structure.

A-C) Immunolabelling on sections of 2DAS seedlings. Immunolabelling is shown in green and cell walls stained with fluorescent brightener 28 are shown in blue. A) JIM19 labelling in Col-0. B) JIM19 labelling in *krs-3*. C) JIM12 immunolabelling on a transverse section of

a Col-0 root. cot = cotyledon, hyp = hypocotyl, eet = extraembryonic tissues of the seed, Scale bars = 100µm in A,B and 50µm in C. D-I) Cuticle staining with auramine 0 on 4 DAS cleared cotyledons. D) Col-0, E) magnification of D, F) *krs-3*, G) magnification of F, H) *gpat4 gpat8*, I) magnification of H. Scale bars = 20µm in D,F,H, = 2µm in E,G,I.

Figure S2: Three independent null alleles of *KRS* show similar phenotypes regarding delay in cotyledon escape and premature seedling growth arrest (Related to Figure 3).

A) Percentage of seedlings with escaped cotyledons at different times after stratification for Col-0 and three null-alleles of *KRS*. N = 3 (repetitions from independent mother plants), 100 seedlings per repetition. Seedling were grown on MS plates supplemented with 0,5% sucrose. The seed batches used in this study was older than the other used in this article. ** represents statistically significant differences (p-value < 0.01) obtained after one-way ANOVA and subsequent Tukey HSD tests. B) Percentage of radicle emergence in the same experiment as that shown in A. +/- SD are represented on each bar plot. C) Quantification of seedling growth arrest (at 12 DAS) in different conditions for Col-0 and three null-alleles alleles of *KRS.*

Figure S3: Variations in water availabilty and pH of growth media affect the cotyledon escape phenotype of *krs* mutants (Related to Figure 3).

A-D) Percentage of seedlings with escaped cotyledons at different times after stratification for Col-0 and *krs-3* lines. N = 3 (repetitions from independent mother plants), 100 seedlings per repetition. Seedlings were grown on MS plates lacking sucrose and with varying concentrations of agarose. A) 0,5% agarose, B) 1% agarose, C) 3% agarose, D) 5% agarose. E-H) Percentage of radicle emergence in the same experiment as that shown in A-D). E) 0,5% agarose, F) 1% agarose, G) 3% agarose, H) 5% agarose. I-K) Percentage of seedlings with escaped cotyledons at different times after stratification for Col-0 and *krs-3* lines. N = 3 (repetitions from independent mother plants), 100 seedlings per repetition. Seedlings were grown on MS plates lacking sucrose and with differing pH. I) pH = 4,0 J) pH = 5,7 (standard condition) K) pH = 8,5. L-N) Percentage of radicle emergence in the same experiment as that shown in I-K). I) pH = 4,0 J) pH = 5,7 (standard condition) K) pH = 8,5. +/- SD are represented on each bar plot.

Figure S4: Supplementary biophysical and microscopic analysis of seedling surface properties (Related to Figure 4).

A) Average adhesion scatter plot on adaxial and abaxial surfaces 2 DAS. Each dot corresponds to the average adhesion measured for 1 cotyledon. Average +/- SEM is indicated on each scatter plot. One-way ANOVA tests were performed between dataset comparisons, with an a-value of 0.05. B) Variability of adhesion maps between cotyledons. Breakdown of adhesion distribution in multiple cotyledons of Col-0, *krs* and *gpat4 gpat8* at 2 DAS. Each dot corresponds to the average adhesion measured for an adhesion map of 64 measurements . Average +/- SEM is indicated on each scatter plot. *** indicates p-value ≤ 0.001, ** indicates p-value ≤ 0.01 and ns indicates p-value > 0,05 in a subsequent Sidak post-hoc test C-H) Comparison of the surfaces of wild-type and *krs* mutants seedlings. C, E, G) Col-0; D, F, H) *krs-3.* C-F) Scanning electron micrographs of cotyledon surfaces 2 DAS. Scale bars = 100µm in C,D) and 10 µm in E,F). G,H) Topographical scans of cotyledon surfaces at 2 DAS obtained using the Atomic Force Microscope. Scales are indicated.

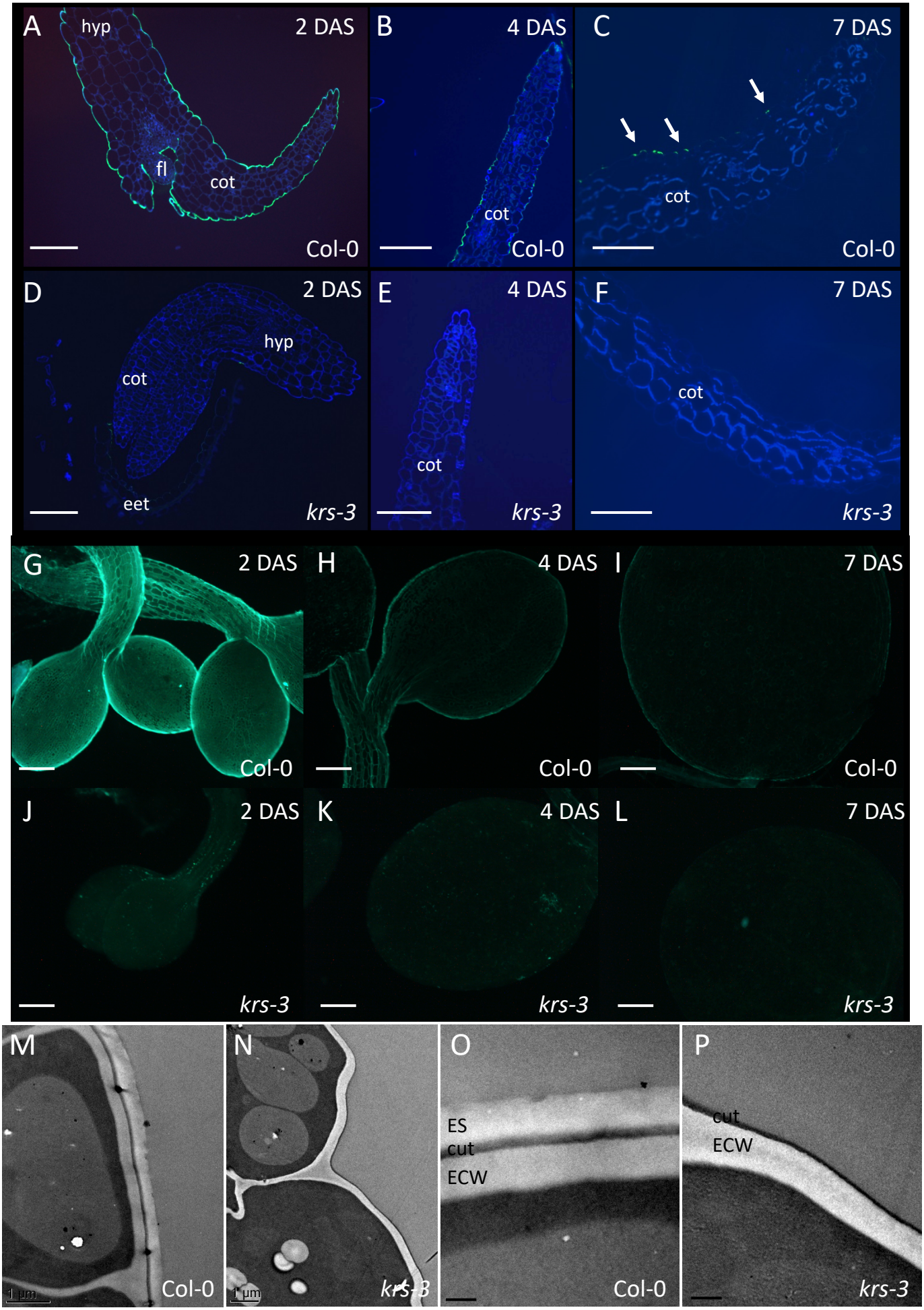
A
hyp
2 DAS
fl
cot
Col-0
B
4 DAS
cot
Col-0
C
7 DAS
cot
Col-0
D
2 DAS
hyp
cot
eet
krs-3
E
4 DAS
cot
krs-3
F
7 DAS
cot
krs-3
G
2 DAS
Col-0
H
4 DAS
Col-0
I
7 DAS
Col-0
J
2 DAS
krs-3
K
4 DAS
krs-3
L
7 DAS
krs-3
M
Col-0
N
krs-3
O
ES
cut
ECW
Col-0
P
cut
ECW
krs-3

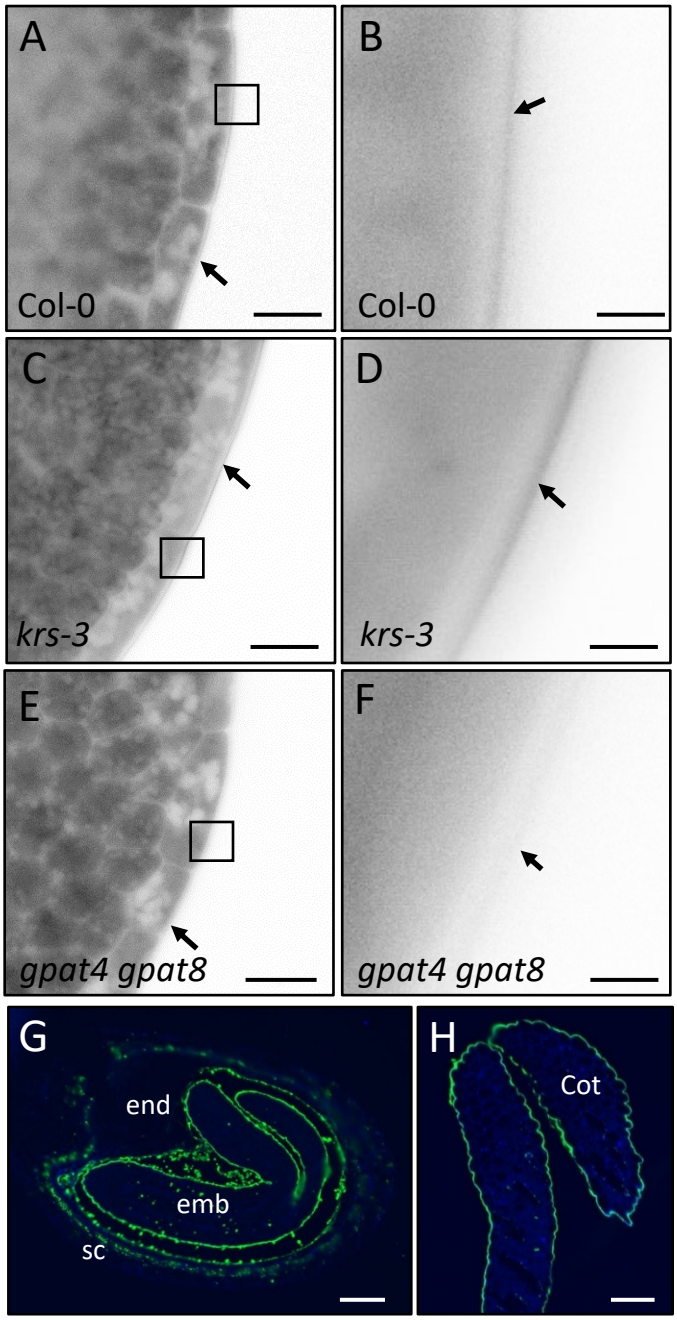
A
Col-0
B
Col-0
C
krs-3
D
krs-3
E
gpat4 gpat8
F
gpat4 gpat8
G
end
emb
sc
H
Cot

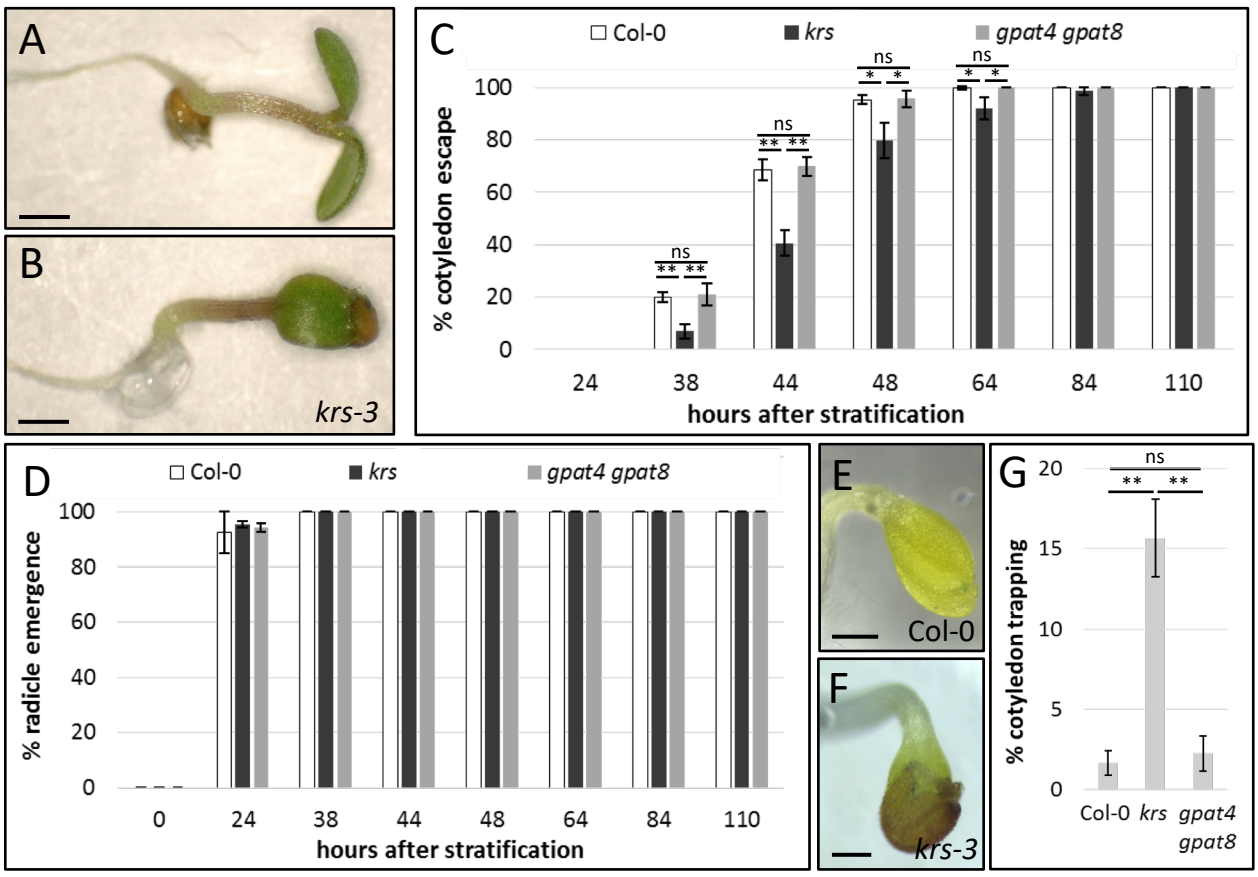
A
B
krs-3
C
Col-0
krs
gpat4 gpat8
% cotyledon escape
hours after stratification
D
% radicle emergence
hours after stratification
E
Col-0
F
krs-3
G
% cotyledon trapping
Col-0
krs
gpat4 gpat8

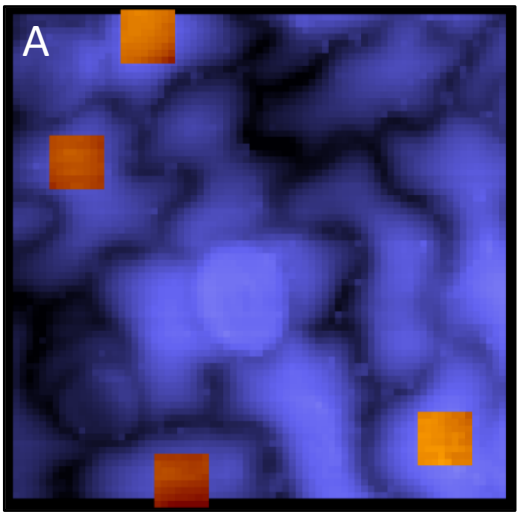
A

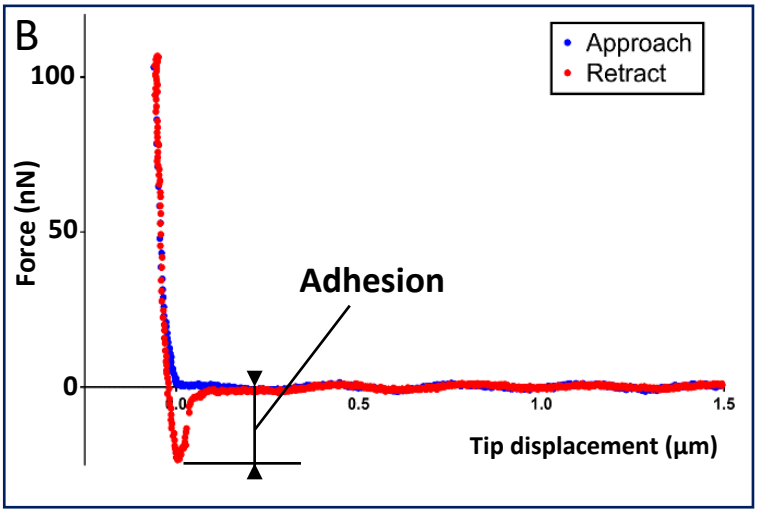
B
Approach
Retract
100
50
0
Force (nN)
Adhesion
0.0
0.5
1.0
1.5
Tip displacement (µm)

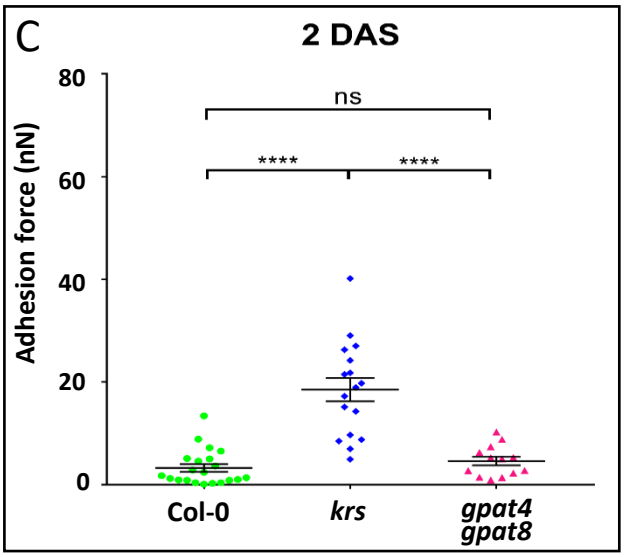
C
2 DAS
Adhesion force (nN)
80
60
40
20
0
ns
****
****
Col-0
krs
gpat4
gpat8

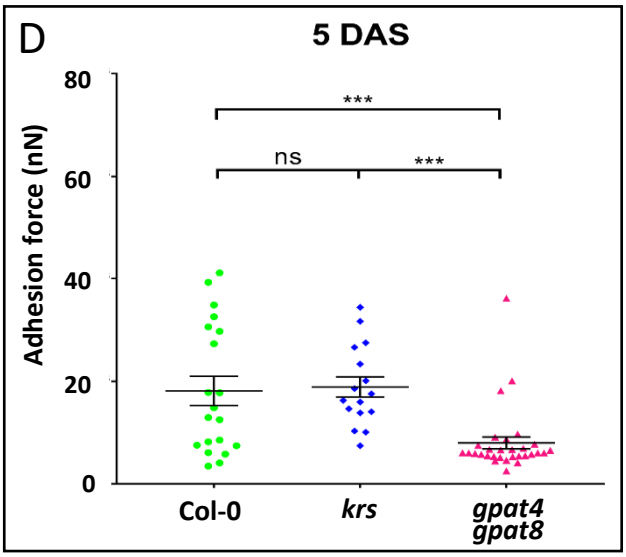
D
5 DAS
Adhesion force (nN)
80
60
40
20
0
***
ns
***
Col-0
krs
gpat4
gpat8

STAR METHODS
LEAD CONTACT AND MATERIALS AVAILABILITY

Further information and requests for resources and reagents should be directed to and will be fulfilled by the Lead Contact, Gwyneth Ingram (gwyneth.ingram@ens-lyon.fr).

This study did not generate new unique reagents.

EXPERIMENTAL MODEL AND SUBJECT DETAILS

Plant materials

The Columbia-0 (Col-0) accession was used as a reference in this study. Three *KRS* loss of function alleles were used, a t-DNA allele (*krs-1*) and two CRISPR lines alleles (*krs-3* and *krs-4*), all described in [2]. The double mutant *gpat4 gpat8* used corresponds to loss of function of both *GPAT4* (*AT1G01610*) and *GPAT8* (*AT4G00400*) by t-DNA insertion and has been described previously [14].

Plant growth

Unless otherwise specified, Arabidopsis seeds were gas-sterilized and sown on MS media (pH = 5,7) with 0.8% Plant agar (Meridis) and 0,5% sucrose and stratified for 2 days at 4°C. Plants were then transferred to long day conditions (16h light) at 21°C.

For generating the seed stocks used, seedlings were transferred to compost (Argile 10 (favorit)) after 7 days, and grown under long day conditions (16h light) at 21°C.

For cotyledon escape tests under light conditions, seeds were sown in rows on MS plates in the presence or absence of sucrose as specified.

For etiolated seedlings, plates were wrapped in aluminium foil for stratification, exposed to a 6h light flash to synchronise germination, re-wrapped and placed in the growth chamber. Observations were carried out in a light free chamber with optional green lighting for observation purposes.

For cotyledon escape tests with varying agarose concentration, 0.5% to 5% of agarose (Sigma-Aldrich) was added to the liquid MS media as specified. For cotyledon escape tests with varying pH, 0.05% w/v of MES hydrate (Sigma-Aldrich) was added to the MS media and pH was adjusted by addition of hydrochloric acid or sodium hydroxide.

For seedling arrest tests, seeds were sown in rows on compost (Argile 10 (favorit)) or on MS plates lacking sucrose, stratified for 2 days at 4°C before transfer to the growth chamber (16h light at 21°C).

For the competition assay, equal weight of *krs-3* and Col-0 seeds (containing a YFP marker expressed in the anthers), were thoroughly mixed and sown at high density on soil. Seeds lots were from mother plants that were grown in identical conditions. The estimated density of seeds on soil was 120 seeds/cm^2. 2 days of stratification were then performed and trays were then transferred to growth chambers. Plants that had bolted after 4 weeks were genotyped by YFP visualisation (Axio Imager 2 microscope (Zeiss)). 3 repetitions of the experiments were performed with seed batches from independent mother plants.

METHOD DETAILS

Germination and cotyledon escape tests

Seeds were grown as described in the previous section. Three batches of 100 seeds, each from independent mother plants, were used as biological replicates. Seeds were observed under a binocular microscope at different times after transfer to the growth chamber and the percentage of radicle emergence and cotyledon escape were recorded. A seedling was considered as showing cotyledon escaped when at least one cotyledon had been released from the seed-coat. Pictures of seedlings in Figure 3 were taken with a Leica MZ12 light microscope.

Cuticle staining

2 DAS and 4 DAS seedlings were fixed with 4% paraformaldehyde (Sigma-Aldrich) in 1X PBS with at least 1 hour of vacuum treatment as described in [24]. Fixed seedlings were then washed twice for 1 min in 1X PBS before being transfer for at least 6-days to ClearSee solution (10% w/v xylitol (Sigma-Aldrich); 15% w/v sodium deoxycholate (Sigma-Aldrich); 25% w/v urea (Euromedex) in water) at room temperature with gentle agitation. Cleared seedlings were then stained with a 0.5% solution of Auramine O (Sigma-Aldrich) in ClearSee. After 12-16 hours of incubation in the dark, seedlings were washed in ClearSee rapidly, then for 30min and then again for at least 1h before being mounted in ClearSee solution. Confocal imaging was performed using a Zeiss LSM700 with a Plan-Apochromat 63x/1,4 oil DIC M27 (ref 420782-9900) objective. Auramine O fluorescence was imaged with a 488nm diode laser excitation and detected with a 505-530nm PMT. Images were then processed using the Zeiss LSM Image Browser Program.

Atomic Force Microscope (AFM)

- **Measurements**

Cotyledons were dissected under a binocular microscope and fixed to the bottom of plastic Petri dishes (Falcon 600 mm x 15 mm, Corning Ref. 351007) using 2-components, bio-compatible glue (Reprorubber-Thin Pour, Flexbar Ref. 16135).

AFM experiments were performed on a stand-alone Nanowizard III microscope (JPK, Bruker), driven by JPK Nanowizard software 6.0. The experiments were performed in filtered MS media (without sucrose) that was used to flood the petri dish as soon as possible after cotyledon immobilisation and 15' to 2 hours before the beginning of the measurements. A silica spherical tip (Special Development SD-sphere-NCH, Nanosensors) mounted on a silicon cantilever with a nominal force constant of 42 N/m, and a radius of 400 nm was used. Cantilevers were cleaned before each experiment in a Hellmanex III (VWR, Ref. 634-0666)/water solution (2% v/v) for 10', then rinsed in water for 10' and finally in ethanol (either pure or 70% solution), in order to remove organic contaminants. This procedure was repeated if there was any suspicion of tip contamination.

Cantilever calibration was performed following the standard thermal noise method. The deflection sensitivity was measured by performing a linear fit of the contact part of a force curve acquired on a sapphire sample in MQ water. The spring constant was determined by acquiring the thermal noise spectrum of the cantilever and by fitting the first normal mode peak using a single harmonic oscillator model. To reduce the offsets in force that introduced by each new calibration, we followed the SNAP protocol developed by [25]. Since the cantilevers used for this study were not independently calibrated by the manufacturer, we considered the spring constant value found at the first calibration as the reference value. In subsequent calibrations, we corrected the deflection sensitivity following SNAP, in order to obtain the same spring constant each time by thermal tune analysis. Then, the new deflection sensitivity and the reference spring constant were set in the instrument's software.

The acquisitions were performed as follows: a first acquisition in Quantitative Imaging (QI) modality at low force (75 nN) and over large areas (90 x 90 μm^2 or 100 x 100 μm^2) gave a first topographic scan for selecting the regions of interest. The first topographic scan was also used to verify that the areas selected were free from contaminants and as flat as possible to minimise tilting of tip-sample contacts. 3 to 4 smaller maps (10 x 10 μm^2, with 8 x 8 force curves) were then acquired in Force Mapping mode, each restricted to 1 single cell. Force curves were acquired with a 4 µm ramp size (2048 data points per curve), with approach and retract speed of 20 µm/s and a force setpoint of 100 nN: This

setpoint is rather small (giving indentations around 50 nm), but high enough to ensure a stable contact for each force curve. Between approach and retract curve, a 2 second pause segment at constant force (100 nN) was imposed, to give a controlled contact time at each point.

- **Data analysis**

Data analysis was carried out using JPK Data Processing software 6.0. Force vs Height Measured curves were first flattened by removing the result of a linear fit performed over a portion of the non-contact part (baseline) of the curve, in order to set this part to a force of 0 N. A first estimation of the point of contact (POC) was obtained, considering it as the first point crossing the 0 of the force, moving backward along the approach curve, starting from its last point (i.e. force setpoint position). The force vs. tip-sample distance curves were then obtained calculating a new axis of distances as Height Measured [m] – cantilever deflection [m].

Adhesion force was measured as the minimum value of force found on the retract segment of the force curve. To filter out spurious adhesion events, the following strategy was used: an RMS value was calculated on a portion of the baseline, then curves were separated into 2 groups depending on whether adhesion passes a threshold value defined as 5 * RMS. This coefficient was selected by visually verifying the correct separation into the 2 groups for several samples. Using a Python routine, an adhesion of 0 nN was assigned to all adhesion events below the previously defined threshold.
Statistical analysis was performed in GraphPad Prism 7.05. For each cotyledon the average of adhesions measured on all the regions of interest defined was calculated. Data were then grouped per genotype and represented as scatter plots, where means +/- SEMs are displayed. T-tests were run if only 2 genotypes were present, for the rest of the comparisons we used one-way ANOVA, comparing each genotype with every other genotype.

Immunolabelling

- **On sections**

Seeds or seedlings were fixed in PEM buffer (15.2g.L-1 PIPES (Sigma-Aldrich), 1.6g.L-1 EGTA (Sigma-Aldrich), 1.2g.L-1 MgSO4,7H2O (MERCK), pH 6.9, in water) containing 4%

(W/V) paraformaldehyde (Sigma-Aldrich) for 1 hour under vacuum, on ice and then overnight at 4°C. Samples were washed 2 times in PEM buffer and dehydrated by incubation in increasing concentrations of ethanol, (50%, 70%, 80%, 90% and three times 100%). Incubations were performed on ice, for one hour and under vacuum. Samples were then infiltrated with increasing concentrations of LR white resin (Euromedex) in absolute ethanol, (30%, 50%, 70% and three times 100%), for 1 hour on ice under vacuum followed by an overnight incubation at 4°C for each bath. Samples were then transferred to small Beam capsules (Electron Microscopy Sciences) and incubated overnight at 60°C for polymerisation. Seed and seedling sections of 1µm were cut on a Leica RM6626 microtome and fixed onto superfrost gold slides (Thermoscientific). For immunolabelling, sections were first incubated for 45 minutes in PBS containing 2% (W/V) of bovine serum albumin (BSA). They were then incubated with a 10-fold dilution of the primary antibody in PBS containing 0.1% (W/V) BSA overnight at 4°C followed by one hour at room temperature. Primary antibodies used for this study were JIM12 and JIM19 (plant probes) [4,26]. Sections are then washed three times in successively PBS for 5 minutes, PBS and 0.1% of tween 20 (W/V) (Sigma-Aldrich) for 10 minutes and PBS for 5 minutes. Incubation with a 1000-fold dilution of anti-rat secondary antibody (AlexaFluor 488 conjugate, Invitogen) in PBS with 0.1% BSA for 1 hour in darkness, in a wet chamber was performed. The sections were washed three times as previously described. Sections were counter-stained with a solution of 0.25 ng.L-1 of calcofluor (Fluorescent Brighter 28 (Sigma Aldrich)) in PBS for 5 minutes. Sections were washed rapidly three times in PBS and mounted in VECTASHIELD solution (Eurobio). Observations were made using an Axio Imager 2 microscope (Zeiss) and images were treated using ImageJ software.

- **Whole mount immunolabelling**

Seedlings were first fixed as described above, then washed two times for 5 minutes in PBS under rotation (30rpm) in 5ml tubes. Immunolabelling was immediately performed using the same protocol as describe above, but with the differences listed below. For the washes, seedlings were put in 5ml tubes with rotation at 30 rpm. For incubation with the primary and the secondary antibodies, the seedlings were carefully transferred to 0.25ml tubes and incubated in 200µL of antibody solution. The counter-staining was not performed and

the seedlings were mounted in water between slide and coverslip. Observations were made using an Imager M2 (Zeiss) microscope images treated using ImageJ software. `

Transmission electron microscopy (TEM)

For TEM analysis, 2 DAS seedlings grown on MS plates with 0,5% sucrose were high-pressure frozen with a Leica EM-PACT-1 system. One or two seedlings were inserted into a flat copper carrier with hexadecene, fast-frozen, and cryosubstituted into the Leica AFS1 device. The different freeze-substitution steps were as follows: 54 h at −90°C in acetone solution containing 0.2% glutaraldehyde (50% aqueous, EMS), 1% osmium tetroxide (EMS), and 0.1% uranyl acetate (EMS). The temperature was then raised with a ramp of 2°C/h before being held for 8 hours at -60°C. The temperature was raised again to -30°C for 8h00 before being increased to 4°C. Samples were washed three times for 10 min in 100% acetone before embedding in Spurr's resin (Spurr Low Viscosity Embedding Kit, Polysciences). Embedding was performed progressively (8 h in 25% Spurr's resin in acetone, one day in 50% Spurr's resin in acetone, one day in 75% Spurr's resin in acetone, and two times overnight in 100% Spurr's resin). Polymerization was performed at 70°C for 18 h.

Samples were sectioned (70 nm sections) on a UC7 Leica ultramicrotome with a diamond knife and imaged at 120 kV using a Phillips CM120 TEM with 2k x 2k Gatan Orius 200 ccd.

QUANTIFICATION AND STATISTICAL ANALYSIS

For all the experiments, detail of statistical tests used and error-bars on barplots are indicated in the figure legends.

DATA AND CODE AVAILABILITY

• This study did not generate/analyze [datasets/code].

REFERENCES

1. Marsollier, A.-C., and Ingram, G. (2018). Getting physical: invasive growth events during plant development. Curr. Opin. Plant Biol. *46*, 8–17.

2. Moussu, S., Doll, N.M., Chamot, S., Brocard, L., Creff, A., Fourquin, C., Widiez, T., Nimchuk, Z.L., and Ingram, G. (2017). ZHOUPI and KERBEROS Mediate

Embryo/Endosperm Separation by Promoting the Formation of an Extracuticular Sheath at the Embryo Surface. Plant Cell *29*, 1642–1656.
3. Smallwood, M., Beven, A., Donovan, N., Neill, S.J., Peart, J., Roberts, K., and Knox, J.P. (1994). Localization of cell wall proteins in relation to the developmental anatomy of the carrot root apex. Plant J. *5*, 237–246.
4. Smallwood, M., Martin, H., and Knox, J.P. (1995). An epitope of rice threonine- and hydroxyproline-rich glycoprotein is common to cell wall and hydrophobic plasma-membrane glycoproteins. Planta *196*, 510–522.
5. Aharoni, A., Dixit, S., Jetter, R., Thoenes, E., Arkel, G. van, and Pereira, A. (2004). The SHINE Clade of AP2 Domain Transcription Factors Activates Wax Biosynthesis, Alters Cuticle Properties, and Confers Drought Tolerance when Overexpressed in Arabidopsis. Plant Cell *16*, 2463–2480.
6. Jenks, M.A., Eigenbrode, S.D., and Lemieux, B. (2002). Cuticular Waxes of Arabidopsis. Arab. Book Am. Soc. Plant Biol. *1*. Available at: https://www.ncbi.nlm.nih.gov/pmc/articles/PMC3243341/ [Accessed March 4, 2019].
7. Para, A., Muhammad, D., Orozco-Nunnelly, D.A., Memishi, R., Alvarez, S., Naldrett, M.J., and Warpeha, K.M. (2016). The Dehydratase ADT3 Affects ROS Homeostasis and Cotyledon Development. Plant Physiol. *172*, 1045–1060.
8. Suh, M.C., Samuels, A.L., Jetter, R., Kunst, L., Pollard, M., Ohlrogge, J., and Beisson, F. (2005). Cuticular Lipid Composition, Surface Structure, and Gene Expression in Arabidopsis Stem Epidermis. Plant Physiol. *139*, 1649–1665.
9. Tanaka, H., Onouchi, H., Kondo, M., Hara-Nishimura, I., Nishimura, M., Machida, C., and Machida, Y. (2001). A subtilisin-like serine protease is required for epidermal surface formation in Arabidopsis embryos and juvenile plants. Development *128*, 4681–4689.
10. Todd, J., Post-Beittenmiller, D., and Jaworski, J.G. (1999). KCS1 encodes a fatty acid elongase 3-ketoacyl-CoA synthase affecting wax biosynthesis in Arabidopsis thaliana. Plant J. Cell Mol. Biol. *17*, 119–130.
11. Bernard, A., and Joubès, J. (2013). Arabidopsis cuticular waxes: advances in synthesis, export and regulation. Prog. Lipid Res. *52*, 110–129.
12. Ingram, G., and Nawrath, C. (2017). The roles of the cuticle in plant development: organ adhesions and beyond. J. Exp. Bot. *68*, 5307–5321.
13. Creff, A., Brocard, L., Joubès, J., Taconnat, L., Doll, N.M., Marsollier, A.-C., Pascal, S., Galletti, R., Boeuf, S., Moussu, S., *et al.* (2019). A stress-response-related inter-compartmental signalling pathway regulates embryonic cuticle integrity in Arabidopsis. PLoS Genet. *15*, e1007847.
14. Li, Y., Beisson, F., Koo, A.J.K., Molina, I., Pollard, M., and Ohlrogge, J. (2007). Identification of acyltransferases required for cutin biosynthesis and production of cutin with suberin-like monomers. Proc. Natl. Acad. Sci. U. S. A. *104*, 18339–18344.
15. Delude, C., Moussu, S., Joubès, J., Ingram, G., and Domergue, F. (2016). Plant Surface Lipids and Epidermis Development. Subcell. Biochem. *86*, 287–313.
16. Verger, S., Long, Y., Boudaoud, A., and Hamant, O. (2018). A tension-adhesion feedback loop in plant epidermis. eLife *7*.
17. Burton, Z., and Bhushan, B. (2005). Hydrophobicity, adhesion, and friction properties of nanopatterned polymers and scale dependence for micro- and nanoelectromechanical systems. Nano Lett. *5*, 1607–1613.
18. Burton, Z., and Bhushan, B. (2006). Surface characterization and adhesion and friction properties of hydrophobic leaf surfaces. Ultramicroscopy *106*, 709–719.

19. Burton, Z., and Bhushan, B. (2006). Surface characterization and adhesion and friction properties of hydrophobic leaf surfaces. Ultramicroscopy *106*, 709–719.
20. Sieber, P., Schorderet, M., Ryser, U., Buchala, A., Kolattukudy, P., Métraux, J.P., and Nawrath, C. (2000). Transgenic Arabidopsis plants expressing a fungal cutinase show alterations in the structure and properties of the cuticle and postgenital organ fusions. Plant Cell *12*, 721–738.
21. Bessire, M., Chassot, C., Jacquat, A.-C., Humphry, M., Borel, S., Petétot, J.M.-C., Métraux, J.-P., and Nawrath, C. (2007). A permeable cuticle in Arabidopsis leads to a strong resistance to Botrytis cinerea. EMBO J. *26*, 2158–2168.
22. Functional analysis of the LACERATA gene of Arabidopsis provides evidence for different roles of fatty acid omega -hydroxylation in development. - PubMed - NCBI Available at: https://www-ncbi-nlm-nih-gov.insb.bib.cnrs.fr/pubmed/?term=Functional+analysis+of+the+LACERATA+gene+of+Arabidopsis+provides+evidence+for+different+roles+of+fatty+acid+omega+-hydroxylation+in+development. [Accessed July 23, 2019].
23. Wellesen, K., Durst, F., Pinot, F., Benveniste, I., Nettesheim, K., Wisman, E., Steiner-Lange, S., Saedler, H., and Yephremov, A. (2001). Functional analysis of the LACERATA gene of Arabidopsis provides evidence for different roles of fatty acid omega -hydroxylation in development. Proc. Natl. Acad. Sci. U. S. A. *98*, 9694–9699.
24. Ursache, R., Andersen, T.G., Marhavý, P., and Geldner, N. (2018). A protocol for combining fluorescent proteins with histological stains for diverse cell wall components. Plant J. Cell Mol. Biol. *93*, 399–412.
25. Schillers, H., Rianna, C., Schäpe, J., Luque, T., Doschke, H., Wälte, M., Uriarte, J.J., Campillo, N., Michanetzis, G.P.A., Bobrowska, J., *et al.* (2017). Standardized Nanomechanical Atomic Force Microscopy Procedure (SNAP) for Measuring Soft and Biological Samples. Sci. Rep. *7*, 5117.
26. Smallwood, M., Beven, A., Donovan, N., Neill, S.J., Peart, J., Roberts, K., and Knox, J.P. (1994). Localization of cell wall proteins in relation to the developmental anatomy of the carrot root apex. Plant J. *5*, 237–246.